Interaction of electronic excitations of Tm^{3+} ions with acoustic vibrations in $KTm(MoO_4)_2$

D. Kamenskyi,[1] S. Poperezhai,[2] P. Gogoi,[1] H. Engelkamp,[1] J. C. Maan,[1] J. Wosnitza,[3] and V. Kut'ko[2]

[1]*Radboud University, Institute for Molecules and Materials, High Field Magnet Laboratory, 6525 ED Nijmegen, Netherlands*

[2]*B. Verkin Institute for Low Temperature Physics and Engineering of the National Academy of Sciences of Ukraine, 47 Lenin Ave., 61103 Kharkov, Ukraine*

[3]*Dresden High Magnetic Field Laboratory (HLD), Helmholtz-Zentrum Dresden-Rossendorf, D-01314 Dresden, Germany*

(Received 10 July 2013; revised manuscript received 25 September 2013; published 13 January 2014)

Electron paramagnetic resonance spectra of $KTm(MoO_4)_2$ were measured as a function of magnetic field between 3 and 11.5 cm^{-1} at $T = 2$ K. We found that in addition to the absorption line caused by the electronic excitation of Tm^{3+} ions, the spectra contain sidebands. Far-infrared transmission measured with polarized light from 10 to 75 cm^{-1} revealed vibration modes at 16.7 and 25.7 cm^{-1} for polarizations $E^{\omega} \parallel a$ and $E^{\omega} \parallel c$, respectively. We show that sidebands in the spectra of paramagnetic resonance result from a parametric resonance between the electronic excitations of the Tm^{3+} ions and the acoustic vibrations of the crystal lattice.

DOI: 10.1103/PhysRevB.89.014410 PACS number(s): 63.20.kd, 71.70.Ej, 76.30.−v, 76.30.Kg

I. INTRODUCTION

$KTm(MoO_4)_2$ belongs to a series of rare-earth compounds with a general formula $MR(MoO_4)_2$, where M^+ is an alkali-metal ion and R^{3+} is a rare-earth ion. The characteristic feature of these materials is the strong coupling between the electronic excitations of the R^{3+} ions and phonons; these electronic excitation energies fit to the lattice-vibrations energies near the maximum in the phonon density of states.[1] Therefore structural phase transitions caused by the Jahn-Teller effect (including those induced by magnetic field) are quite frequent in these compounds.[2–7]

In this paper, we discuss $KTm(MoO_4)_2$ for which previous measurements of the magnetic susceptibility and the specific heat have shown that neither structural phase transitions nor magnetic ordering occur down to 0.1 K.[8] The absence of the phase transitions may be caused by competition of magnetic and Jahn-Teller interactions of paramagnetic Tm^{3+} ions. Such an effect has been observed in compounds of this family containing R^{3+} ions with an even numbers of f electrons.[9,10]

The lowest multiplet of the non-Kramers Tm^{3+} ions, $^3H_6$, is split by the crystal field to 13 $(2J + 1)$ singlets. The energy separation of the lowest levels is usually too large to be observed by electron paramagnetic resonance (EPR). However, previous investigations on $KTm(MoO_4)_2$ revealed that the first Stark level is 2.3 cm^{-1} above the ground state; for the next level, this is 200 cm^{-1}.[8,11] Thus this compound can be considered to be an almost ideal quantum two-level system at low temperatures. It was shown that the low-energy quasidoublet formed by these levels have the maximum possible M_J values: $|M_J\rangle = |\pm\rangle J = |\pm 6\rangle$. In magnetic fields, the quasidoublet splits further. The g factor of this splitting is very large ($g_c = 13.9$) for fields aligned parallel to c and $g_{a,b} \approx 0.4$ for fields along a and b.[12]

An external magnetic field applied along the c axis shifts the electronic excitations of Tm^{3+} towards higher energies until they coincide with phonon energies. This gives a unique possibility to investigate the dynamic of electron-phonon interactions by varying the strength of an externally applied magnetic field. We investigated far-infrared (FIR) transmission and EPR over a broad range of frequencies. Since the electronic excitations of Tm^{3+} ions are strongly localized, the electron-phonon interaction determines the structure of the electronic level identically throughout the Brillouin zone. Thus measurements of the microwave absorption at the center of the Brillouin zone give us information on the coupling to phonons over the complete zone.

II. EXPERIMENTAL DETAILS

Single crystals of $KTm(MoO_4)_2$ were grown from a melt by slow cooling. The crystallographic structure has the space group P_{bcn} (D_{2h}^{14}) with the lattice constants $a = 5.05$ Å, $b = 18.28$ Å, $c = 7{,}89$ Å, and four formula units per unit cell.[13,14] It consists of $[Tm(MoO_4)_2]^-$ layers which are built from MoO_4 tetrahedra and TmO_8 octahedra and are separated by layers of K^+ ions (see Fig. 1). The weak bonding between the layers along the b direction is responsible for the thin plates crystal shape. Important is that the K^+ ions are bonded to one of the $[Tm(MoO_4)_2]^-$ layers within cell somewhat stronger than to another one.[13]

The samples investigated had typical dimensions of $9 \times 5 \times 0.2$ mm^3. This allows to measure the transmission spectra with the polarizations $E^{\omega} \parallel a$ and $E^{\omega} \parallel c$ axes (E^{ω} is electric component of the microwave radiation).

FIR transmission spectra were measured using a commercial Fourier-transform infrared spectrometer (Bruker IFS113v) combined with a continuous-field 33-T Bitter magnet at 1.4 K at the High Field Magnet Laboratory in Nijmegen.[15] A mercury lamp was used as a radiation source. The FIR radiation was detected using a silicon bolometer operating at 1.4 K below the field center with a maximal field <7 T. The data were collected between 10 and 75 cm^{-1} with 0.1 cm^{-1} resolution using a 200-μm mylar beamsplitter and a scanning velocity of 50 kHz. At each field, at least 50 scans were averaged.

The EPR measurements were performed at the Dresden High Magnetic Field Laboratory[16] using a transmission-type spectrometer[17] over the frequency range 3–11.5 cm^{-1} (90–345 GHz) at $T = 2$ K. Virginia Diodes Inc. microwave sources were employed as radiation sources. The microwave radiation propagated along the b axis of the crystal. The external magnetic field (H) was applied along the c axis, which corresponds to the highest g factor.

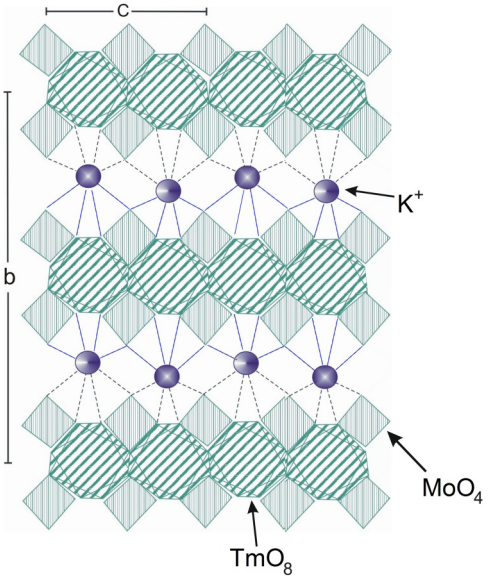

FIG. 1. (Color online) Crystallographic structure of $KTm(MoO_4)_2$ projected on the bc plane. Dashed and solid lines between the K^+ ions and the $[Tm(MoO_4)_2]^-$ layers are supposed to represent weaker and stronger bonds, respectively.

III. RESULTS

The FIR transmission spectra of $KTm(MoO_4)_2$ at 1.4 K are shown in Fig. 2. We found absorption peaks at 16.7 and 25.7 cm^{-1} for polarizations $E^\omega \parallel a$ and $E^\omega \parallel c$, respectively (arrows in Fig. 2). Standing waves within the plane-parallel sample cause interference in the spectra, which is visible as a Fabry-Perot type modulation of the transmittance in Fig. 2.

Figure 3 shows EPR spectra of $KTm(MoO_4)_2$ at different frequencies. We found an intensive absorption peak (marked by A in Fig. 3), which corresponds to the transition within the lowest quasidoublet with a zero-field gap of 2.33 cm^{-1}. The ground state of such systems is described by the conventional non-Kramers doublet spin Hamiltonian for an effective spin

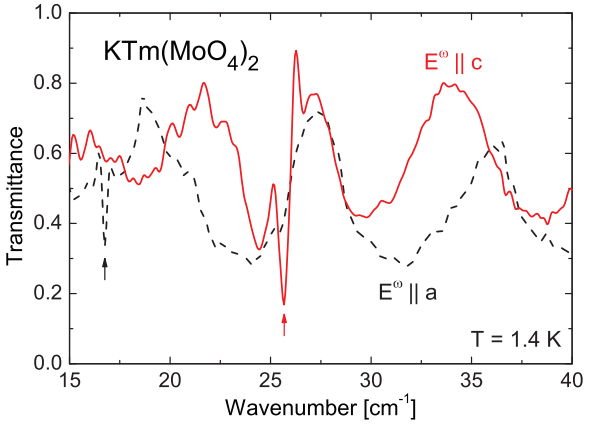

FIG. 2. (Color online) Transmission spectra of $KTm(MoO_4)_2$ at polarizations $E^\omega \parallel a$ (dashed black) and $E^\omega \parallel c$ (solid red). Arrows show absorption peaks.

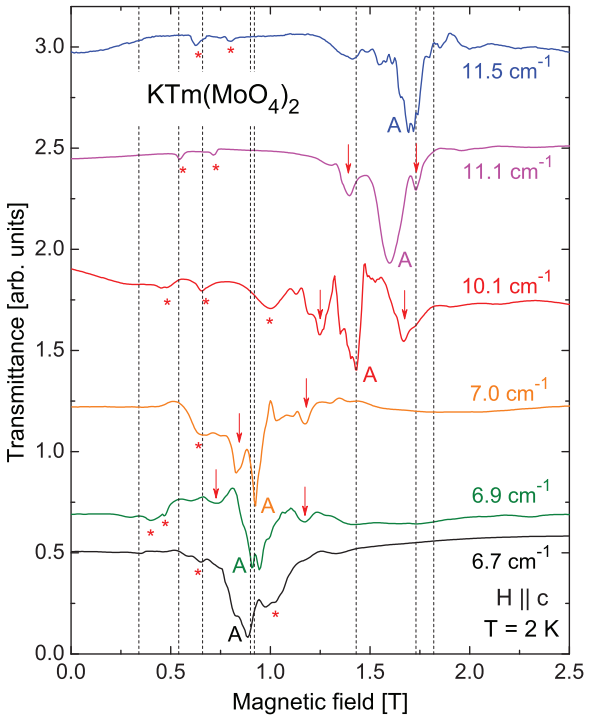

FIG. 3. (Color online) EPR spectra of $KTm(MoO_4)_2$ at different frequencies for H $\parallel$ c and $T = 2$ K.

$S = 1/2$:[18]

$$\mathcal{H} = g_z \mu_B H_z S_z + \Delta_x S_x + \Delta_y S_y. \quad (1)$$

The terms $\Delta_x S_x$ and $\Delta_y S_y$ are induced by the crystal field. They lead to a zero-field energy gap $\Delta = [\Delta_x^2 + \Delta_y^2]^{1/2}$ and mix the two lowest nondegenerate states. This mixing allows transitions within non-Kramers doublet when the oscillating magnetic field, H^ω, has a parallel component along the z direction ($H^\omega \parallel H$).[18] Such an effect is not unique for Tm^{3+} ions. Similar EPR properties were reported for Tm^{3+} in a multicomponent fluorozirconate glass.[19]

The frequency-field dependence of the peak A is shown in Fig. 4. Red points show data obtained by EPR, blue points by the FIR setup. The black line corresponds to a fit using the

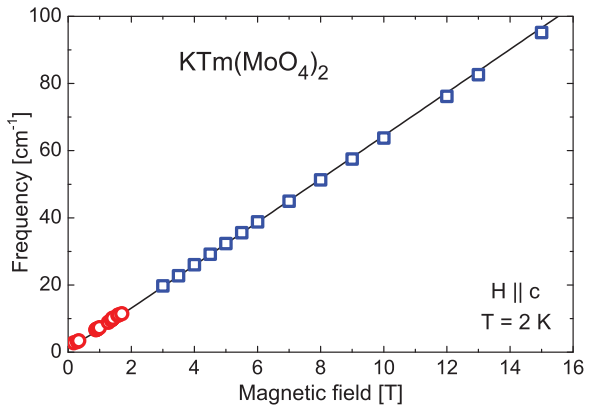

FIG. 4. (Color online) Frequency-field dependence of the peak A. Red circles are data obtained by EPR, blue squares by the FIR setup.

formula

$$\hbar\omega_0 = [\Delta^2 + (g\mu_B H)^2]^{1/2}, \quad (2)$$

where ω_0 is the radiation frequency. The values obtained for $g \sim 13.8$ and $\Delta \sim 2.33$ cm^{-1} are in agreement with previous EPR investigations.[12]

At some frequencies, sidebands of the peak A appear (shown by arrows in Fig. 3). Additionally, a number of weak absorptions marked by asterisks have been observed. At some frequencies, the peak A splits (6.9, 10.1, 11.5 cm^{-1}) and the intensity of the anomalies increases (10.1 cm^{-1}). Since the sidebands are situated quite far from the main resonance peak A, they cannot be explained by the electrodynamic effects near the resonance, e.g., by a change in the sample's refractive index. In the following, we argue that the observed features in the EPR spectra are caused by the dynamic coupling between the electronic excitations of Tm^{3+} ions and the lattice vibrations.

IV. DISCUSSION

FIR acoustic spectra of $KR(MoO_4)_2$ compounds are formed by the shear vibrations of the $[R(MoO_4)_2]^-$ layer as a whole along different crystallographic directions.[1,20] Thus, the dispersion of the vibration branches in the Brillouin zone, $\omega_{ph}(k)$, can be calculated using a one-dimensional model. The dispersion relation of the vibrational branches of a linear chain with two masses ($M > m$) is well-known:

$$\omega_{ph}^2 = \alpha(1/m + 1/M) \pm \alpha[(1/m + 1/M)^2 - 4\sin^2(ka/2)/mM]^{1/2}, \quad (3)$$

where α is the shear force constant, $\omega = 2\pi\nu$ is the angular frequency, a is the lattice parameter, and k is the quasi-wave-vector.[21] Plus and minus correspond to the optical and acoustic branches, respectively.

$KTm(MoO_4)_2$ forms two nonequivalent layers, $[Tm(MoO_4)_2]^-$ and $([Tm(MoO_4)_2]^- + 2K^+)$, because, as it has been mentioned above, the K^+ ions are bonded to one of the $[Tm(MoO_4)_2]^-$ layers within cell stronger than to another one (see Fig. 1).[13] Thus, due to folding of the Brillouin zone, new low-frequency optical branches appear. Physically, they represent shear vibrations $[Tm(MoO_4)_2]^-$ versus $([Tm(MoO_4)_2]^- + 2K^+)$ layers, and are observed by us as the FIR absorption peaks at 16.7 and 25.7 cm^{-1} (see Fig. 2) for the a and c axes, respectively.

The frequency of the optical branch at $k = 0$:

$$\omega_{opt} = [2\alpha(1/m + 1/M)]^{1/2}, \quad (4)$$

where M and m mases of $[Tm(MoO_4)_2]^- + 2K^+$ and $[Tm(MoO_4)_2]^-$ layers, respectively. We used the obtained frequencies of the optical modes to determine α from Eq. (4) and calculate the dispersion of these modes, $\omega_{ph}(k)$, using Eq. (3). The results of calculations are shown in Fig. 5.

The sideband structure observed in the EPR spectra (see Fig. 3) can now be explained by resonant dynamic coupling between the electronic excitations of Tm^{3+} ions and the lattice vibrations. The resonant dynamic coupling of these excitations is possible if the following conditions are met: (a) the electronic and phonon excitations must be of identical symmetry and (b) the interacting excitations must have equal energies and wave vectors.

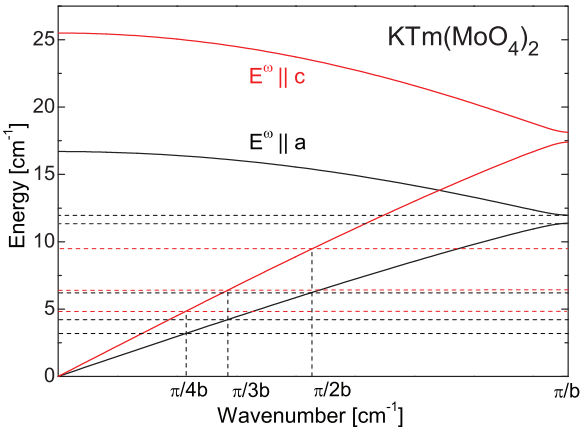

FIG. 5. (Color online) Dispersion of acoustic and optic vibration branches of $KTm(MoO_4)_2$. The horizontal dashed lines correspond to the energies of phonons with wavelengths multiple of the lattice constant.

The excitation spectrum of Tm^{3+} ions is determined by their local symmetry, and the low-frequency vibration excitations are dependent on the symmetry of the crystal. To check whether condition (a) is fulfilled it is necessary to find out the compatibility of the irreducible representations of the corresponding symmetry groups. The local symmetry group of Tm^{3+} ions is C_2 and the factor group is D_{2h}. Table I contains the irreducible representations of the local symmetry group of Tm^{3+} ions and the factor group. The irreducible representations of the symmetry group of the electronic excitations Γ_1, Γ_2 are compatible with the representations $\Gamma_1^+, \Gamma_1^-, \Gamma_2^+, \Gamma_2^-$ and $\Gamma_3^+, \Gamma_3^-, \Gamma_4^+, \Gamma_4^-$ of the factor group, respectively. Vibrations shown in Fig. 5 have the odd symmetry Γ_2^-, Γ_3^-, Γ_4^-. Thus the coupling between the Tm^{3+} ions electronic excitations of symmetry Γ_1, Γ_2 and the odd-symmetry lattice vibrations Γ_2^-, Γ_3^-, Γ_4^- is allowed. The EPR spectra have been measured at $k \parallel b$, i.e., with $E^\omega \perp C_2$ axis (the local symmetry C_2 axis of Tm^{3+} is parallel to the b axis), which is an excitation of the symmetry Γ_2 compatible with the representations Γ_3^-, Γ_4^-. These representations characterize the transverse acoustic vibrations of the $[Tm(MoO_4)_2]^-$entities within the layer.

The lattice vibrations modulate the crystal field on the Tm^{3+} sites. It leads to a modulation of the zero-field gap, Δ, in Eq. (2). Usually, such a dynamic electron-phonon coupling leads to a broadening of the EPR absorption peak.[22] In $KTm(MoO_4)_2$, we found that the electron-phonon coupling is resonant and induce nonlinear effects. The phonon energies are quite low and coincide with the energies of electronic excitations at certain magnetic fields. It leads to parametric resonance between electronic excitations and phonons.

TABLE I. The compatibility of irreducible representation of the symmetry group C_2 and the factor group D_{2h}.

C_2	Γ_1	Γ_2
D_{2h}	Γ_1^+ Γ_1^- Γ_2^+ Γ_2^-	Γ_3^+ Γ_3^- Γ_4^+ Γ_4^-

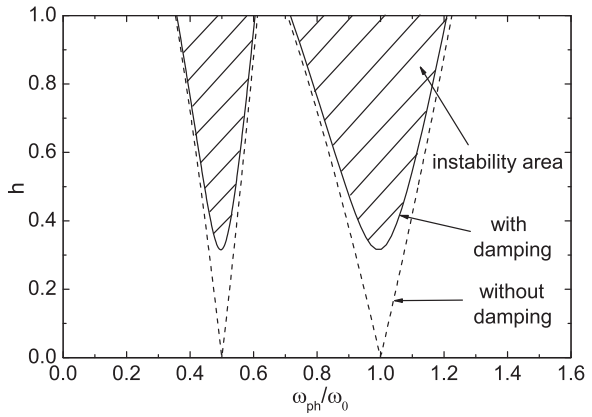

FIG. 6. Stability diagram of the Mathieu equation for $n = 1,2$ (see text). Inside the hatched area, the Eq. (5) has no stable solution.

Parametric oscillator is described by the Mathieu equation. In the simple case of a pendulum in a time-dependent gravitational field:[23]

$$\frac{d^2\Theta}{dt^2} + \gamma\frac{d\Theta}{dt} + \omega_0^2[1 + h\cos(2\omega t)]\Theta = 0, \qquad (5)$$

where Θ is an angular variable, γ is the damping factor, ω_0 is the eigenfrequency of the pendulum, h is the relative amplitude of the modulation, and ω is the modulation frequency. The solutions of Eq. (5) are given by transcendental functions, called Mathieu functions, which we do not describe further. It is very important that Eq. (5) has stable solutions at certain conditions only. For an undamped system ($\gamma = 0$), the theory predicts instabilities at $\omega_0/\omega = 1/n$ (n is integer). Such instabilities result in parametric resonances of the system. Figure 6 shows the stability diagram of Eq. (5) equation for $n = 1,2$.

In our case, the electronic excitations play the role of the pendulum and the lattice vibrations are the external modulation. One can see in Fig. 6 that if the frequency of the electronic excitations, ω_0, coincide with the modulation frequency, ω_{ph}, and the amplitude of the modulation is strong enough, Eq. (5) has no stable solution and the amplitude of the oscillations increases. The modulation amplitude enhances when the energies of the electronic excitations coincide with phonon energies of wavelengths that are a multiple of the lattice constant (shown by vertical dashed lines in Fig. 5). The lattice vibrations with these wavelengths form standing waves and nodes are localized at weak interlayer bonds. Thus neighboring $[Tm(MoO_4)_2]^-$ layers move in antiphase, which modulates the crystal-field most strongly at the Tm^{3+} sites. This leads to a resonant enhancement of the dynamic electron-phonon coupling and induces splitting and inhomogeneous broadening of the EPR peak.

The horizontal dashed lines in Fig. 5 show the energies of the acoustic phonons with wavelength of a multiple of the lattice constant (3.2, 4.2, 4.8, 6.3, 6.4, 9.5, 11.4, and 12.0 cm^{-1}). Using the calculated phonon frequencies and Eq. (2), we can estimate the resonance magnetic fields for electronic excitations of same energy (0.33, 0.54, 0.66, 0.90, 0.92, 1.43, 1.73, and 1.83 T). When the resonance field is close to calculated fields (shown by vertical dashed lines in Fig. 3) the system falls into the instability area (see Fig. 6). It leads to the splitting of peak A and a very asymmetrical shape of it (see spectra at 6.9, 10.1, and 11.5 cm^{-1} in Fig. 3). We believe that the additional features in spectra at 6.9, 10.1, and 11.5 cm^{-1} are induced by nonlinear modulation of electronic excitation energy.

Since ω_0 is magnetic field dependent according to Eq. (2), the dynamic electron phonon coupling can be varied by the field. Outside the instability area, the EPR spectrum becomes noiseless and the sidebands appear (see the spectrum at 11.1 cm^{-1} in Fig. 3). The parametric modulation in Eq. (5) leads to a low frequency modulation of the electronic excitation if system is close to instability area.[24] It induces the sideband structure in the EPR spectra. The positions of the sidebands in the spectra are determined by the modulation frequency. Since the solutions of the Eq. (5) are strongly field-dependent, the positions of the sidebands are asymmetric respect to peak A. The sidebands in FIR spectra induced by electron phonon coupling reported also for other $KR(MoO_4)_2$ compounds.[1] We found the sideband structure survive in instability area as well (shown with arrows in Fig. 3).

Thus, in $KTm(MoO_4)_2$, we have the unique possibility to control the dynamic electron-phonon interaction by magnetic field. However, the strong field dependence of this coupling makes interpretation of the EPR spectra challenging. Additionally, the resonant parametric coupling is expected not only when the frequencies coincide, but also at the subharmonics of the lattice vibrations.[24] This may lead to an additional structure of weak absorptions in EPR spectra (marked by asterisks in Fig. 3).

V. CONCLUSIONS

We investigated the transmission spectra of $KTm(MoO_4)_2$ by use of FIR and EPR techniques. Evidence of the parametric resonance between electronic excitations of Tm^{3+} ions and acoustic phonons in form of sidebands has been observed in EPR signal. This nonlinear effect is induced by the dynamic electron-phonon interaction. We have shown that the electron-phonon coupling is enhance when the electronic level of Tm^{3+} ions crosses the vibration branches with wave vectors multiples to the lattice constant.

The observation of the parametric resonance suggests $KTm(MoO_4)_2$ as a good model compound for the study of the nonlinear dynamical effects by varying the magnetic field and the microwave radiation power. At fields when the coupling is strong enough and the excitation energies coincide, the system may exhibit further nonlinear behavior when the radiation power is increased.

ACKNOWLEDGMENTS

This work is part of the research program of the Foundation for Fundamental Research on Matter (FOM), which is part of the Netherlands Organisation for Scientific Research (NWO). Parts of this work were supported by EuroMagNET II (contract No. 228043) and EMFL (contract No. 26211). The authors would like to thank A. V. Pronin, S. A. Zvyagin, and M. F. Kharchenko for fruitful discussions.

[1]V. I. Kut'ko, Fiz. Nizk. Temp. **31**, 3 (2005) [Low Temp. Phys. **31**, 1 (2005)].
[2]A. I. Zvyagin, T. S. Stetsenko, V. G. Yurko, and R. A. Vaishnoras, JETP Lett. **17**, 135 (1973).
[3]A. I. Zvyagin, S. D. El'chaninova, T. S. Stetsenko, L. N. Pelikh, and E. N. Khats'ko, Fiz. Nizk. Temp. **1**, 79 (1975) [Sov. J. Low Temp. Phys. **1**, 39 (1975)].
[4]M. J. M. Leask, A. C. Tropper, and M. R. Wells, J. Phys. C. **14**, 3481 (1981).
[5]S. Matas, E. Dudzik, R. Feyerherm, S. Gerischer, S. Klemke, K. Prokes, and A. Orendacova, Phys. Rev. B **82**, 184427 (2010).
[6]C. Detlefs, F. Duc, Z. A. Kazei, J. Vanacken, P. Frings, W. Bras, J. E. Lorenzo, P. C. Canfield, and G. L. J. A. Rikken, Phys. Rev. Lett. **100**, 056405 (2008).
[7]V. I. Kut'ko and M. I. Kobets, Fiz. Nizk. Temp. **22**, 1447 (1996) [Low Temp. Phys. **22**, 1099 (1996)]; Czech. J. Phys. 46, Suppl. **5**, 2555 (1996).
[8]V. A. Pashchenko, V. G. Borisenko, E. N. Khats'ko, A. S. Cherny, C. Paulsen, A. Feher, M. Orendác, A. Orendácová, A. G. M. Jansen, and P. Wyder, J. Phys.: Condens. Matter **14**, 9693 (2002).
[9]B. G. Vekhter and M. D. Kaplan, Fiz. Tverd. Tela **15**, 2013 (1973).
[10]A. H. Cooke, S. J. Swithendy, and M. R. Wells, J. Phys. C **6**, 2209 (1973).
[11]M. I. Kobets, V. S. Kurnosov, V. A. Pashchenko, and E. N. Khats'ko, Fiz. Nizk. Temp **25**, 512 (1999) [Low Temp. Phys. **25**, 379 (1999)].
[12]V. A. Pashchenko, A. G. M. Jansen, M. I. Kobets, E. N. Khats'ko, and P. Wyder, Phys. Rev. B **62**, 1197 (2000).
[13]V. I. Spitsin and V. K. Trunov, Dokl. Akad. Nauk SSSR **185**, 854 (1969) (in Russian).
[14]B. M. Wanklyn and F. R. Wondre, J. Cryst. Growth **43**, 93 (1978).
[15]S. A. J. Wiegers, P. C. M. Christianen, H. Engelkamp, A. den Ouden, J. A. A. J. Perenboom, U. Zeitler, and J. C. Maan, J. Low Temp. Phys. **159**, 389 (2010).
[16]J. Wosnitza, T. Herrmannsdörfer, Y. Skourski, S. Zherlitsyn, S. A. Zvyagin, O. Drachenko, H. Schneider, and M. Helm, AIP Conf. Proc. **1003**, 311 (2008).
[17]S. A. Zvyagin, J. Krzystek, P. H. M. van Loosdrecht, G. Dhalenne, and A. Revcolevschi, Physica B **346–347**, 1 (2004).
[18]A. Abragam and B. Bleaney, *Electron Paramagnetic Resonance of Transition Iions* (Clarendon press, Oxford, 1970), p. 209.
[19]E. A. Harris and D. Furniss, J. Phys.: Condens. Matter **3**, 1889 (1991).
[20]J. Hanuza and L. Macalic, Spectrochim. Acta A **38**, 61 (1982); J. Hanuza, L. Macalik, and K. Hermanowicz, J. Mol. Struct. **319**, 17 (1994).
[21]H. J. Pain, *The Physics of Vibrations and Waves* (Wiley, England, 2005), p. 139.
[22]A. Abragam and B. Bleaney, *Electron Paramagnetic Resonance of Transition Ions* (Clarendon press, Oxford, 1970), p. 557.
[23]P. Berge, Y. Pomeau, and C. Vidal, *Order within Chaos* (Wiley, New York, 1986), p. 35.
[24]P. Berge, Y. Pomeau, and C. Vidal, *Order within Chaos* (Wiley, New York, 1986), p. 34.